Macromolecules

# When Microrheology, Bulk Rheology, and Microfluidics Meet: Broadband Rheology of Hydroxyethyl Cellulose Water Solutions

Francesco Del Giudice,*,[†] Manlio Tassieri,*,[‡] Claude Oelschlaeger,[¶] and Amy Q. Shen[†]

[†]Micro/Bio/Nanofluidics Unit, Okinawa Institute of Science and Technology Graduate University, 1919-1 Tancha, Onna-son, Kunigami-gun, Okinawa, 904-0495 Japan

[‡]Division of Biomedical Engineering, School of Engineering, University of Glasgow, Glasgow G12 8LT, U.K.

[¶]Institute for Mechanical Process Engineering and Mechanics, Karlsruhe Institute of Technology (KIT), Gotthard-Franz-Strasse 3, 76131 Karlsruhe, Germany
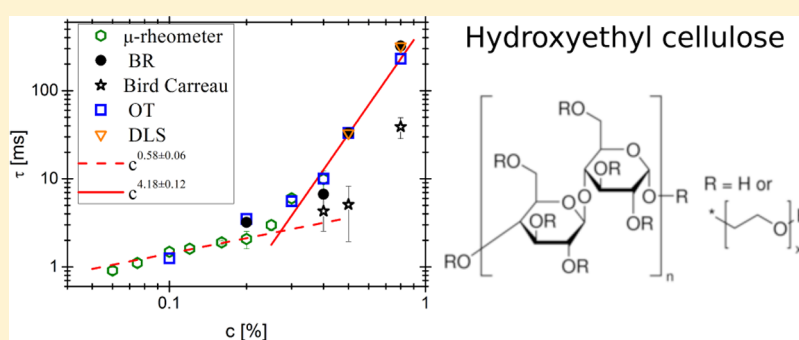
ABSTRACT: In this work, we present new insights related to a debate on the morphological structure of hydroxyethyl cellulose (HEC) molecules when dissolved in water, i.e., whether HEC adopts a linear-flexible or a rod-like fibrillar configuration. We have employed "seven" rheological techniques to explore the viscoelastic properties of HEC solutions at different time and length scales. This work demonstrates an excellent convergence between various rheological techniques over a broad range of frequencies and concentrations, allowing us to derive microstructural information for aqueous HEC solutions without the use of complex optical imaging techniques. We find that when dissolved in water unmodified HEC behaves like a linear uncharged polymer, with an entangled mass concentration of $c_e = 0.3$ wt%. Moreover, for the first time we provide the concentration scaling laws (across c_e) for the longest relaxation time λ of HEC solutions, obtained from *direct* readings and not inferred from fitting procedures of fluids shear flow curves.

1. INTRODUCTION

Cellulose is the most abundant biological material on earth. Hydroxyethyl cellulose (HEC) is obtained from the chemical reaction of ethylene oxide with cellulose.[1] Thanks to its high solubility in water, HEC is widely used in various industrial and biomedical applications.[2−5] For example, it is widely used as a thickening agent in paints,[6−9] textiles,[5,9,10] membrane preparations,[11,12] drug delivery,[13−18] and tissue engineering.[19−22] Nevertheless, despite its importance in industrial processing, the rheological properties of HEC solutions are still not well understood, and HEC morphology in solution remains a matter of debate.

While the majority of rheological studies[1,19,23,24] agree on the non-Newtonian nature of aqueous HEC solutions (i.e., that they exhibit shear-thinning behavior, especially at relatively high HEC concentrations and shear rates), it is unclear whether HEC in water is a flexible linear polymer[1,23−27] or a rod-like fibril.[28]

Solutions containing different microstructural variants tend to exhibit very different rheological properties, both in terms of concentration-dependent (zero-shear) viscosities and their frequency-dependent viscoelastic properties, as shown by the pioneering studies of Doi and Edwards.[29,30]

In this work, we have investigated aqueous HEC solutions by employing "seven" different rheological techniques, each able to explore the viscoelastic properties of HEC at different length scales, including (i) conventional bulk-rheology using a stress-controlled rotational rheometer;[31] microrheological methods (ii) optical tweezers (OT),[32−38] (iii) diffusing wave spectroscopy (DWS),[39,40] (iv) dynamic light scattering (DLS),[41,42] and (v) multiple particle tracking (MPT)[43−48] plus two microfluidics platforms (vi) m-VROC[49,50] (section 2.4.1) and (vii) the μ-rheometer[51,52] (section 2.4.2). Results from all these techniques agree remarkably well over a broad range of concentrations and frequencies, allowing us (i) to reveal the viscoelastic nature of aqueous HEC solutions and (ii) to educe the concentration scaling laws governing the longest relaxation
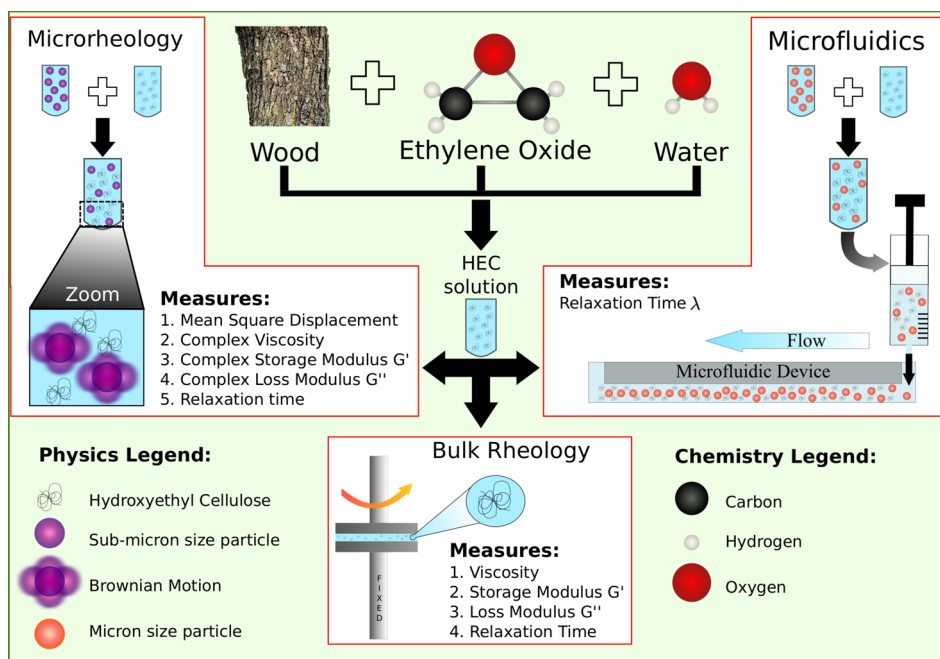
Figure 1. Hydroxyethyl cellulose is obtained from the chemical reaction of ethylene oxide with wood-based cellulose. The solution can be characterized through different rheological techniques. Bulk rheology (bottom) is performed to measure the macroscopic fluid's viscoelastic properties such as the shear viscosity, storage and the loss moduli. Microrheology (left) is based on the observation of free or driven motion of tracer particles introduced into the fluid under investigation. In particular, the mean square displacement is evaluated, from which rheological parameters can be derived.[62,63] Microfluidics technique (right) is used to measure the longest fluid shear relaxation time by counting the number of particles aligned on the channel centerline at a fixed distance from the channel inlet.[51]

time of unmodified HEC solutions in semidilute unentangled and semidilute entangled regimes.

2. THEORETICAL AND EXPERIMENTAL BACKGROUND

2.1. Current Understanding of HEC Solutions. Despite the fact that HEC is widely used for a variety of applications (Figure 1), the rheological properties of aqueous HEC solutions remain controversial.[25,28,53,54] Hoffmann et al.[53] concluded that HEC is an uncharged linear polymer, even though their results at low concentrations (in the dilute regime) agreed with theoretical scaling laws for polyelectrolyte solutions. They reasoned that this was due to charges on the HEC molecule. Nevertheless, at higher HEC concentrations (in the semidilute regime), their results followed theoretical predictions for uncharged linear polymers,[55] where interactions among charges were screened by the presence of other polymer chains. Similar conclusions were drawn by Laschet et al.,[25] who reported that solutions of HEC behaved like those of uncharged linear polymers, obeying the extended Huggins equation.[56] Their findings are in agreement with many others.[1,23,24,26,27]

Interestingly, recent works[28,54] have offered new insights on the viscoelastic nature of HEC solutions. By means of a chemical process, Saito et al.[57] extracted cellulose microfibrils (with length ranging from nanometers to micrometers) from HEC. Subsequently, Ishii et al.[54] characterized solutions of such HEC microfibrils, finding that HEC solutions behaved like those of rod-like polymer solutions. Similar rheological observations were reported recently on fibrous and nanocrystalline cellulose.[58−61] Arfin and Bohidar[28] captured scanning electron microscope (SEM) images and rheologically characterized HEC solutions with different molecular weights. They confirmed the presence of HEC microfibrils even without chemical treatment. However, their rheological studies agree well with theoretical predictions developed for solutions of random coil polymers.[55] Moreover, bear in mind that SEM images are taken of dried samples, and caution must be taken when comparing results obtained from wet samples.

2.2. Conventional Bulk Shear Rheometry. Rheology is the study of matters in flow. Conventionally, rheological studies focus mainly on mechanical properties of complex fluids (e.g., polymer melts) under flow. Thanks to the continuous development of theoretical models,[29,64,65] relating the frequency-dependent linear viscoelastic properties (LVE) of materials to their molecular structures and dynamics, linear rheological measurements have proven invaluable for gathering microstructural information on samples at different length scales.[66,67]

The LVE properties of a material can be represented by its frequency-dependent complex shear modulus $G^*(\omega) = G'(\omega) + iG''(\omega)$; where ω is the angular frequency, i is the imaginary unit (i.e., $i^2 = -1$), and $G'(\omega)$ and $G''(\omega)$ are the material storage (elastic) and loss (viscous) moduli, respectively. Conventionally, linear bulk rheology measurements are performed by means of a stress-controlled (or strain-controlled) rotational rheometer, where a sinusoidal stress (or strain) is applied and the resulting strain or stress of the material is measured. These measurements are commonly limited (i) in the range of accessible high frequencies because of the instrument inertia (with a maximum value on the order of 100 Hz) and (ii) by the sensitivity required to measure very low viscosity fluids,[35] as well as (iii) the sample volume required to perform the measurement (on the order of milliliters), which is a limiting factor when materials are available only in small quantities (precious materials).[68]

Modern microrheology[41,69] and microfluidic[50,51,70] techniques have significantly extended the range of experimentally accessible frequencies (or time scales). This is mainly due to the micron length scales at which the measurements are performed (i.e., low inertia), but also thanks to the high sampling rate of modern detectors.

2.3. Microrheology. Microrheology is underpinned by the same principles that govern classical rheology, but experiments and information are obtained at micron length scales.[69] The most popular microrheology techniques involve passive video particle tracking (PVPT),[71,72] multiple particle tracking (MPT),[46−48] magnetic tweezers (MT),[73,74] optical tweezers (OT),[32−35,75] dynamic light scattering (DLS),[76] diffusing wave spectroscopy (DWS)[39,40] and atomic force microscopy (AFM).[77,78] More recent microrheological

Table 1. $G^*(\omega)$ Expressions for Different Microrheology Techniques: Passive Video Particle Tracking (PVPT),[71,72] Multiple Particle Tracking (MPT),[46−48] Magnetic Tweezers (MT),[73,74] Optical Tweezers (OT),[32−35,75] Dynamic Light Scattering (DLS)[76] and Diffusing Wave Spectroscopy (DWS)[39,40] [a]

technique	measured parameter	complex modulus relationship
PVPT and MPT	tracer trajectory $r(t)$	
DLS	tracer MSD $\langle \Delta r^2(\tau) \rangle$	$\pi a G^*(\omega)/(k_B T) = [i\omega\langle \widehat{\Delta r^2}(\omega)\rangle]^{-1}$
DWS	tracer MSD $\langle \Delta r^2(\tau) \rangle$	
MT	tracer trajectory $r(t)$	$6\pi a G^*(\omega)/F_E = [i\omega\hat{r}(\omega)]^{-1}$
OT	tracer trajectory $r(t)$	$6\pi a G^*(\omega)/\kappa = \hat{A}(\omega)/\hat{\Pi}(\omega)$

[a]Here $\langle \widehat{\Delta r^2}(\omega)\rangle$ is the FT of the particles' mean-square displacement (MSD) $\langle \Delta r^2(\tau)\rangle = \langle [r(t+\tau) - r(t)]^2\rangle$. $\hat{\Pi}(\omega)$ and $\hat{A}(\omega)$ are the FTs of $\Pi(\tau)$ and $A(\tau)$, which are the normalized mean-square displacement (NMSD)[75] $\Pi(\tau) = \langle \Delta r^2(\tau)\rangle/2\langle r^2\rangle$ and the normalized position autocorrelation function (NPAF)[88] $A(\tau) = \langle r(t)\, r(t+\tau)\rangle/\langle r^2\rangle$, respectively.

techniques include:[79] laser-deflection particle tracking,[80] particle interferometric tracking,[81,82] confocal particle tracking,[83,84] and angular light streak particle tracking.[85] With the exception of AFM, these techniques are all based on the measurement of the motion of tracer particles introduced into the fluid under investigation. In particular, there are two broad classes of microrheology techniques: (I) those measuring the *passive* motion of particles due to thermal (Brownian) fluctuations of molecules in solution, and (II) those involving *active* manipulation of probes by means of an externally applied force field. Both classes of methods directly relate time-dependent tracer trajectory ($\mathbf{r}(t)$) to the frequency-dependent LVE properties of the suspending fluid.

In particular, when a micron-sized spherical particle is immersed in a fluid at thermal equilibrium, it experiences random forces due to thermal fluctuations of the surrounding fluid's molecules. For freely diffusing particles, the statistical mechanics study of their trajectories can provide information on the viscoelastic properties of the suspending fluid.[62] Similarly, when the particle motion is constrained or driven by an external applied force (e.g., a harmonic potential generated by the optical tweezers), the particle trajectory can be described by applying a generalized Langevin equation similar to that introduced by Weitz and Mason,[62] but with an extra term $F_E(t)$ accounting for the external force acting on the particle:

$$m\mathbf{a}(t) = \mathbf{F}_R(t) - \int_0^t \boldsymbol{\zeta}(t-\tau)\mathbf{v}(\tau)\, \mathrm{d}\tau + \mathbf{F}_E(t) \tag{1}$$

where m is the mass of the particle, $a(t)$ is its acceleration, $v(t)$ is its velocity and $F_R(t)$ is the usual Gaussian white noise term, modeling stochastic thermal forces acting on the particle. The integral term represents the viscous damping by the fluid. This is defined as the convolution between the particle velocity and a generalized time-dependent memory function $\boldsymbol{\zeta}(t)$, that embodies the viscoelastic nature of the fluid. For instance, in the case of optical tweezers, $F_E(t) = -kr(t)$, where k is the stiffness of the optical trap.

In general, it has been shown[62,74,86,87] that eq 1 (with or without $F_E(t)$) can be solved to find $G^*(\omega)$ in terms of the Fourier transform (FT) of either the particle position ($\hat{r}(\omega)$) or one of the related time-averaged functions, shown in Table 1. In Table 1, the inertia term ($m\omega^2$) reported in the original expressions[62,74,86−88] has been disregarded because for micron-sized particles it becomes significant only at frequencies on the order of megahertz.

2.4. Microfluidic Rheometry. 2.4.1. Viscosity Measurement. Measurements of fluids' viscosity by means of capillary viscometers have become a standard procedure for rheological studies as soon as the measurement of high shear rate become achievable.[31] The same principles can be transferred to micrometer length scales, once an accurate measure of the pressure drop Δp in the microchannel is fulfilled.[49,50] The highest shear rate achieved in a micrfluidic device depends on the onset of fluid dynamic instabilities in the micro-channel,[49] which occurs at $\dot{\gamma} \sim 10^4 − 10^5\ \mathrm{s}^{-1}$, for low viscosity fluids. The lowest shear rate depends on the diameter of the syringe used to pump the fluid, on the pumping system itself, and on channel dimensions.[49] Generally, for low viscosity fluids (with a viscosity value of the order of $\eta \sim 10^{-3} − 10^{-1}$ Pa·s), such as dilute and semidilute

aqueous polymer solutions, the lowest shear rate is $\dot{\gamma} \sim 10^{-3} − 10^1\ \mathrm{s}^{-1}$, respectively. Notably, when combined, microfluidic- and bulk rheology enable rheological characterization of the fluids over a wide range of shear rates.

For these measurements, the wall shear stress σ_{wall} and the apparent wall shear rate $\dot{\gamma}_{wall,app}$ in a rectangular channel are defined as[49]

$$\sigma_{wall} = \frac{WD\Delta p}{2L(W+D)} \tag{2}$$

$$\dot{\gamma}_{wall,app} = \frac{6Q}{WH^2} \tag{3}$$

where W is the channel width, H is the channel height, Q is the imposed flow rate, and L is the distance between the inlet of the capillary channel over which the pressure drop Δp is measured.

Notice that, for Newtonian fluids the apparent shear rate $\dot{\gamma}_{wall,app}$ is equivalent to the true shear rate $\dot{\gamma}_{wall}$; whereas, for viscoelastic fluids the true shear rate is obtained through the well-known Weissenberg−Rabinowitsch correction:[31]

$$\dot{\gamma}_{wall} = \frac{\dot{\gamma}_{wall,app}}{3}\left[2 + \frac{d(\ln \dot{\gamma}_{wall,app})}{d(\ln \sigma_{wall})}\right] \tag{4}$$

The true viscosity is then measured as

$$\eta(\dot{\gamma}_{wall}) = \frac{\sigma_{wall}}{\dot{\gamma}_{wall}} = \frac{WD\Delta p}{2L(W+D)}\frac{1}{\dot{\gamma}_{wall}} \tag{5}$$

The microfluidic platform used in this work for measuring the shear viscosity of HEC solutions is called m-VROC (RheoSense, Inc.).

2.4.2. Longest Relaxation Time Measurement. Even though m-VROC is a very precise tool for measuring the shear viscosity of fluids, it is unable to directly measure the fluid's longest relaxation time λ. This can be inferred by employing the Bird Carreau model,[89] which adopts λ as a fitting parameter of the viscosity shear flow curve. An alternative and direct measurement of λ has been made possible thanks to novel microfluidic platforms,[51,90] including the recently developed μ-rheometer.[91] The μ-rheometer is able to reveal λ by observing the transverse migration of micrometer-scale particles in a Poiseuille flow.[91−95] The working principle of the μ-rheometer can be summarized as follows: when micron-sized particles suspended in a Newtonian liquid flow at low flow rates (i.e., in inertialess fluid dynamic conditions) in a straight channel, they can only follow the streamlines in the direction of the flow due to the reversibility of the Navier−Stokes equations.[96] The scenario changes for a viscoelastic fluid. In particular, the polymer chains act as small springs that, when deformed by the Poiseuille flow, generate an elastic force able to push the suspended particles toward either the channel centerline[91] or the corners of a square-shaped microchannel.[95] In order to reach those positions, particles must migrate across the streamlines. Dynamics of the transverse migration toward the centerline is governed by a single dimensionless parameter:[97]

$$\Theta = De \frac{L}{H} \beta^2 \tag{6}$$

where L is the distance from the channel inlet, H is the characteristic length of the channel, $\beta = D_p/H$ is the confinement ratio (with D_p the particle diameter), $De = k\lambda\dot{\gamma}_c$ is the Deborah number, which contains the fluid's shear relaxation time λ and a characteristic shear rate $\dot{\gamma}_c$. The value of the parameter k depends on the unit of λ. In particular, $k = 1$ for $\lambda = [\text{s/rad}]$; whereas, $k = 1/2\pi$ for $\lambda = [\text{s}]$. In this work, we use $k = 1$ because the values of λ obtained from the μ-rheometer have been compared with those extrapolated from the linear viscoelastic response of the HEC solutions at different concentrations, where $\omega = [\text{rad/s}]$.

As described in Del Giudice et al.,[95] the fraction of particles aligned at the centerline, f_1, is given by

$$f_1 = \frac{1}{1 + Be^{-C\Theta^2}} \tag{7}$$

which is an interpolating analytical expression of the theoretical model depicting the transverse migration of particles in straight channels, with constants values of $B = 2.7$ and $C = 2.75$ obtained as best curve fit parameters.[95] By measuring the fraction of particles aligned on the channel centerline at a distance L from the inlet position, the parameter Θ can easily be evaluated and so λ via eq 6. Notice that, based on the underlying assumptions of the theoretical model, eq 7 is only valid when (i) $\Theta < 1$, i.e. generally for small De (values of $De \sim 0.1-0.5$ have been previously used[95,97]) and (ii) small confinement ratio $\beta = d_p/H \sim 0.1$, where d_p is the particle diameter. Once these conditions are satisfied, eq 7 represents a *universal relation*. In this work, we have used a square-shaped μ-rheometer, where the characteristic length is the channel height H, and the characteristic shear rate is $\dot{\gamma}_c = 4\,Q/H^3$. The shear relaxation time λ can be derived from the inversion of eq 7:

$$\lambda_{shear} = \frac{1}{\beta^2}\frac{H^4}{LQ}\sqrt{\frac{1}{C}\ln\left(\frac{f_1 B}{1 - f_1}\right)} \tag{8}$$

2.5. Concentration Scaling Laws for Flexible and Rod-Like Polymer Solutions. We now review the concentration scaling laws for flexible[55] and rod-like[98,99] polymer solutions. We focus on the scaling laws of shear viscosity and relaxation time as a function of polymer concentration only, because the polymer molecular weight of HEC is kept as a constant in our study.

2.5.1. Flexible Polymer Solutions. For flexible polymers, we highlight the existence of four concentration regimes, within which the shear viscosity and the relaxation time follow defined power laws with respect to polymer concentration and solvent quality. Different solvent qualities lead to different polymer conformations in solution.[100] These four regimes are identified as follows: (i) the *dilute* regime at concentration $c < c*$ ($c*$ the so-called *overlapping concentration*), where the polymer chains do not interact with each other; (ii) the *semidilute unentangled* regime at concentrations $c* < c < c_e$ (c_e the so-called *entanglement concentration*), where polymer chains start interacting hydrodynamically; (iii) the *semidilute entangled* regime at concentrations $c_e < c < c**$, where polymer chains are "loosely" entangled; and finally, (iv) the *entangled* regime for concentrations $c > c**$, where the polymer chains are "tightly" entangled.

Concentration scaling laws of viscosity within these regimes are also able to reveal important information about the "quality" of the solvent by means of the dimensionless scaling exponent ν. In particular, a value of $\nu = 0.5$ corresponds to the so-called θ-solvent, a value of $\nu = 0.6$ defines a *good solvent*, while a value of $\nu = 1$ represents polyelectrolytes without salt.[55] Different values of ν identify the three universality classes for polymer solutions.[100] Moreover, the value of ν does not depend on the polymer regime investigated.[55]

We now show the concentration scaling laws for the specific viscosity η_{sp_0} of the polymer solution at zero-shear rate, which is defined as follows:

$$\eta_{sp_0} = \frac{\eta_0}{\eta_s} - 1 \tag{9}$$

where η_0 is the zero-shear viscosity of the polymer solution and η_s is the solvent viscosity. The concentration scaling laws of η_{sp_0} and λ in the *semidilute unentangled* regime are described as[55]

$$\eta_{sp_0} \propto c^{1/(3\nu-1)} \quad \text{and} \quad \lambda \propto c^{(2-3\nu)/(3\nu-1)} \tag{10}$$

For the *semidilute entangled* regime they are

$$\eta_{sp_0} \propto c^{3/(3\nu-1)} \quad \text{and} \quad \lambda \propto c^{3(1-\nu)/(3\nu-1)} \tag{11}$$

A full discussion on scaling laws in flexible polymer solutions can be found in the book of Rubinstein and Colby[100] or in Colby.[55]

2.5.2. Rod-Like Polymer Solutions. For rod-like polymer solutions, scaling laws do not depend on solvent quality through the dimensionless parameter ν, because only rod-like configuration exists in solution. Despite their importance in soft-matter physics, biology and industrial processing, the viscoelastic properties of semiflexible (rod-like) polymer solutions are still not well understood and a basic analytical model has not yet been agreed upon; as recently corroborated by Schuldt et al.[101] Nevertheless, in the case of rod-like polymers (with a persistence length much bigger than the contour length), three polymer concentration regimes are generally acknowledged:[98] (i) the *dilute* regime, where rod-like polymers do not interact with each other; (ii) the *semidilute or entangled* regime where rod-like polymers are entangled with each other; (iii) the *concentrated* regime, where rod-like polymers can be oriented, leading to the so-called *nematic phase*.[98]

The concentration scaling laws for the specific viscosity η_{sp_0} in the *dilute* and *semidilute* regimes are[98]

$$\eta_{sp_0,D} \propto c \quad \text{and} \quad \eta_{sp_0,SD} \propto c^3 \tag{12}$$

with obvious meaning of the subscripts.

In the *concentrated* regime, theoretical predictions of general validity cannot be formulated, because of the occurrence of the material's phase transition from isotropic to nematic state. The linear viscoelastic properties of the latter are material dependent, and therefore can change case by case.

Interestingly, within the above two concentration regimes, λ is either not defined or independent by the polymer concentration, respectively. Indeed, in the *dilute* regime, the presence of rod-like polymers affects only the (Newtonian) viscosity of the solvent (because of the increase of contact area between the polymer and the solvent), but not the solution's dynamics (because the polymer molecules (i) cannot be deformed (rod-like) and (ii) are diluted). Whereas, in the *semidilute* (entangled) regime, λ depends only on the polymer molecular weight (i.e., rod length) and not on its concentration.[98,99]

3. MATERIALS AND METHODS

3.1. Materials. Hydroxyethyl cellulose with a nominal average molecular weight of $M_w = 250$ kDa was purchased from Sigma-Aldrich. The value of $M_w = 250$ kDa has been "estimated" by the manufacturer from their viscosity measurements. Here, we perform our own characterization of the polymer. We conducted dynamic light scattering measurements (LS Instruments, AG) and measured the polymer's average molecular weight M_w, its radius of gyration R_g and the second virial coefficient A_2 by means of a Zimm plot.[102] The sign of A_2 represents either repulsion ($A_2 > 0$) or attraction ($A_2 < 0$) between chains. When $A_2 > 0$ the solution is stable, but when $A_2 < 0$, polymer chains can aggregate, leading to phase separation.[100]

The Zimm plot is obtained from light scattering measurements on dilute polymer solutions at different angles. We carried out dynamic light scattering measurements (section 3.5) on HEC solutions from 0.005 to 0.03 wt%. For each concentration, we explored five scattering angles from 30° to 110°, with 20° increment. For each angle, we performed three independent measures, each of duration of 180 s

(chosen based on the longest measuring time required to derive the autocorrelation function at the smallest angle). The materials' parameters can be derived from the following equation:[102]

$$\frac{Kc}{\Delta R(c,\theta)} = \frac{1 + \frac{q^2 R_g^2}{3}}{M_w(1 + 2cA_2)} \tag{13}$$

where c is the polymer concentration, K is an optical constant depending on the refractive index increment dn/dc with n the refractive index, θ is the scattering angle, ΔR is the excess Rayleigh ratio (i.e., the difference between the Rayleigh ratio of the solution and that of a standard fluid; in this case, Toluene), and q is the scattering vector. The refractive index increment $dn/dc = 0.14$ ml/g has been measured on the same set of HEC solutions with an Anton Paar Abbemat refractometer. The Zimm plot is obtained by plotting $\frac{Kc}{\Delta R(c,\theta)}$ versus $q^2 + \phi c$, where ϕ is a shifting factor determined by the software accompanying the DLS instrument. Once the measurements are performed, the DLS software fits the data and extrapolates the values at $c = 0$ and $\theta = 0$ to obtain the aimed parameters (Figure 2). The
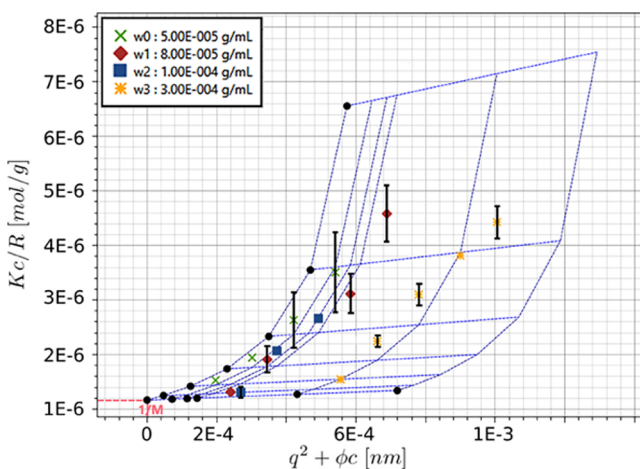

Figure 2. Zimm plot for aqueous HEC solutions. Different points represent different polymer concentrations. Blue lines are the extrapolations to $c = 0$ and $\theta = 0$, with c the polymer concentration and θ the scattering angle. The scattering angle is contained in the wave vector q, and ϕ is a shifting factor determined by the software. The measured parameters are $M_w = 850$ kDa, $R_g = 65$ nm, and $A_2 = 1.77 \times 10^{-4}$ mol·mL/g^2.

resulting values are $M_w = 850$ kDa, $R_g = 65$ nm, and $A_2 = 1.77 \times 10^{-4}$ mol·mL/g^2 (with $A_2 > 0$ indicating a stable system). Our value of R_g is in good agreement with $R_g = 69$ nm found by Vadodaria and English[103] from rheological measurements on HEC with $M_w = 720$ kDa, while our value of A_2 is in rather good agreement with $A_2 = 4.3 \times 10^{-4}$ mol·mL/g^2 determined by Brown et al.[104] from light scattering measurements on HEC 600 kDa in water at 25 °C. Given the significant difference between the nominal and the DLS measured value of the HEC molecular weight, we decided to compare these values with the one derived from our rheological measurements (Figure 4) via the Mark–Houwink equation, which relates the *intrinsic viscosity*[31] $[\eta] = \lim_{c\to 0} (\eta_{sp_0}/c)$ to the molecular weight of the polymer. For HEC in water, the Mark–Houwink relation is[26]

$$[\eta] = 7.4 \times 10^{-3} \times M_w^{0.89} \tag{14}$$

with $[\eta]$ expressed in mL/g. We found $[\eta] = 1034 \pm 220$ mL/g and $M_w = 604 \pm 143$ kDa, which is closer to the one obtained from the Zimm plot, than the value estimated by the manufacturer. Finally, the persistence length for HEC in water has been reported[105,106] as $10 < l_p < 30$ nm.

Our rheological investigations employed aqueous solutions of HEC at mass concentrations ranging from 0.05 wt% to 7 wt%. Solutions

were stirred at 200 rpm for 48 h at room temperature. The obtained solutions were transparent, and no aggregates were observed. All experiments were carried out within 2 weeks of initial sample preparation to prevent sample degradation.

3.2. Bulk Rheology Measurements. Rheological measurements were performed by using a stress-controlled rotational rheometer MCR 302 (Anton Paar Instrument) with the lowest torque values of ∼0.1 μNm. The measurements were performed with a cone and plate geometry with 50 mm in diameter and 1° angle. Experiments were performed at a temperature of 22 °C and the rheometer was equipped with a solvent trap to avoid fluid evaporation.

3.3. Optical Tweezer Measurements. Optical trapping was achieved with a titanium-sapphire laser with a 5 W pump (Verdi V5 laser; Coherent Inc.), which provides up to 1 W at 830 nm. The optical tweezer system is built on an inverted microscope, where the same objective lens (100x, 1.3 numerical aperture, Zeiss, Plan-Neofluar) is used for both focusing the trapping laser beam and visualizing the thermal fluctuations of a single 5 μm diameter silica bead. Samples were mounted on a motorized microscope stage (Prior Pro-Scan II). A CMOS camera (Dalsa Genie HM640 GigE) was used to collect high-speed images of a reduced field of view. These images were processed in real time at ∼1 kHz using homemade LabVIEW (National Instruments) single-particle-tracking software[107] running on a personal computer. Note that each trajectory represents at least 10^6 data points. Experiments were performed at 22 °C.

3.4. Diffusive Wave Spectroscopy Measurements. Diffusive wave spectroscopy (DWS) measurements were performed by using a commercially available instrument (DWS-rheolab, LS Instruments AG). The DWS-rheolab uses a diode laser module with a wavelength of 685 nm and an output power of 40 mW. This machine analyses laser fluctuations generated by the collective Brownian motion of concentrated particle suspensions. Particles with diameter $d_p = 0.4$ μm (MicroParticle GmbH) were suspended in the HEC solution at a particle concentration of 1 wt%. The sample was loaded in the standard sample cell with length of 2 mm. A calibration curve with water was performed in the same sample cell, and at the same particle concentration used for HEC solutions. The autocorrelation function was converted in $G'(\omega)$ and $G''(\omega)$ by using the method of Mason.[63] Experiments were performed at 22 °C.

3.5. Dynamic Light Scattering Measurements. Dynamic light scattering DLS measurements were performed with a 3D LS spectrometer from LS Instruments AG. The scattering angle can vary from 20° to 155°. This method is based on the analysis of the laser fluctuations generated by the collective Brownian motion of dilute particle suspensions. Particles with diameter $d_p = 0.4$ μm (MicroParticle GmbH) were suspended in the HEC solutions at a volume particle concentration of 0.001 vol %. The autocorrelation function was measured at an angle of 30° and then converted into $G'(\omega)$ and $G''(\omega)$ via the method of Mason.[62] Experiments were performed at 22 °C.

3.6. Multiple Particle Tracking. Multiple particle tracking based optical microrheology (MPT) experiments were performed using an inverted fluorescence microscope (Axio Observer D1, Zeiss), equipped with a Fluar 100×, N.A. 1.3, oil-immersion lens combined with a 1× Optovar magnification changer. We tracked the Brownian motion of green fluorescent polystyrene microspheres of 0.5 μm (Bangs Laboratories) used as tracer particles. Images of these fluorescent beads were recorded on a personal computer using an sCMOS camera Zyla X (Andor Technology: 21.8 mm diagonal sCMOS sensor size, 2160 × 2160 pixels). Displacements of particle centers were monitored in a 127 × 127 μm field of view, at a rate of 50 frames/s. Movies of the fluctuating microspheres were analyzed by a custom MPT routine incorporated into the software Image Processing System (Visiometrics iPS) and a self-written Matlab program[47] based on the widely used Crocker and Grier tracking algorithm.[108] Additionally, to perform statistical analyses and to characterize the microstructure heterogeneity, we examined the distribution of displacements, known as the Van Hove correlation function[109,110] given by

$$G_s(r, \tau) = \frac{1}{N}\left\langle \sum_{i=1}^{N} \delta[r + r_i(0) - r_i(\tau)]\right\rangle = \frac{N(r, \tau)}{N} \qquad (15)$$

where $r_i(\tau)$ is the distance traveled by a particle i in a time τ. $N(r, \tau)$ is the number of particles that move a distance between r and $(r + dr)$ in a time interval τ, and N is the total number of particles. If all particles are exposed to similar environment, $G_s(r, \tau)$ has a Gaussian form. Deviations from this form reflect the presence of heterogeneities, and can be characterized by the non-Gaussian parameter α:[110]

$$\alpha = \frac{\langle x^4(\tau)\rangle}{3\langle x^2(\tau)\rangle^2} - 1 \qquad (16)$$

This quantity is zero for a Gaussian distribution, while deviations from this distributions can result in a large α value.

3.7. Microfluidic-Based Measurements. Two different microfluidic platforms were used to characterize the fluid rheology: (i) m-VROC from Rheosense, Inc. and (ii) homemade μ-rheometer. The first device was used for measuring the shear viscosity of HEC solutions at high shear rates, whereas the μ-rheometer was used to measure the fluid's longest shear relaxation time.

The m-VROC consists of a microfluidic channel with several pressure sensors being placed along the channel. The fluid is pumped inside the channel (depth $h = 100~\mu m$, made of pyrex mounted on a gold-coated silicon base) at an imposed flow rate and the pressure drop is measured.

The μ-rheometer is made of a straight square-shaped microfluidic channel (lateral side $H = 100~\mu m$, made of PolyMethylMethacrylate). The channel is milled on the PMMA substrate using a micromilling machine (Minitech CNC Mini-Mill) following a procedure reported previously.[91] After fabrication, the channel is bonded onto another PMMA substrate by immersing the two pieces in absolute ethanol (from Sigma-Aldrich) for ~20 min, clamping them together, and putting the device into an oven at $T = 40~°C$ for about 2 h. Polystyrene particles with $D_p = 10~\mu m$ are suspended in each of the fluid investigated, at a volume fraction $\phi = 0.01\%$.

4. RESULTS AND DISCUSSION

In principle, when different rheological techniques are employed for measuring the material's linear viscoelastic properties, their results should either be identical (if the investigations are performed over the same range of frequency) or should overlap over a discrete region of frequencies, so that the overall outcome of the rheological study would be "self-consistent". Unfortunately, these conditions are rarely satisfied in literature when bulk- and microrheology measurements are compared.[111,112]

In the following, we present results obtained from linear and nonlinear bulk-rheology, passive microrheology and microfluidic rheology, which show remarkable agreements and allow us to reveal new insights on the morphology of HEC in aqueous solutions.

4.1. Viscosity Curve. In order to explore the non-Newtonian nature of HEC solutions, we first investigated how shear viscosity (η) varies as a function of the shear rate $\dot{\gamma}$ for HEC solutions at different mass concentrations. In particular, we have measured the viscosity curves over a wide range of shear rates (see Figure 3) by employing two complementary rheometers: a conventional rotational shear rheometer and a m-VROC device. Notice that, in Figure 3 we have displayed only a few selected viscosity curves, to ensure a better visualization and critical analysis.

Figure 3 shows that at relatively low HEC mass concentrations (i.e., for $c < 0.3$ wt%), solutions behave almost like a Newtonian fluids in the range of shear rates investigated, $10^0 < \dot{\gamma} < 10^4~s^{-1}$. At relatively higher concentrations (i.e., for c
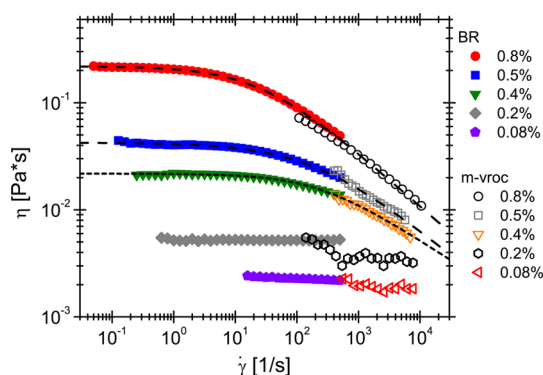

Figure 3. Viscosity flow curves for HEC solutions at different mass concentrations. Filled symbols indicate bulk rheology measures (BR) made with a rotational rheometer. Open symbols indicate viscosity values of HEC solutions measured experiments by means of an m-VROC device. Dashed lines are the best fit of the viscosity curves using the Bird–Carreau model.[89]

> 0.3 wt%) they exhibit a typical non-Newtonian (i.e., shear-thinning) behavior, where viscosity curves start with a plateau region at low $\dot{\gamma}$ and then drop at relatively high shear rates, as reported in literature by others.[1,23,24,26,27] The microscale m-VROC device enables us to reach the high shear rate ($500 < \dot{\gamma} < 10^4~s^{-1}$) regime without encountering inertial effects. It becomes possible to estimate the zero-shear viscosity (η_0) of each HEC solution with concentration $c > 0.3$ wt% by fitting the related viscosity flow curve with the Bird–Carreau model.[89] Measuring η_0 reliably allows us to evaluate the specific viscosity at zero-shear (η_{sp_0}, see eq 9), which then can be adopted not only to identify different concentration regimes (Figure 4), but also to discriminate between different structures adopted by the polymer in solution (coil-like or rod-like), as described hereafter.
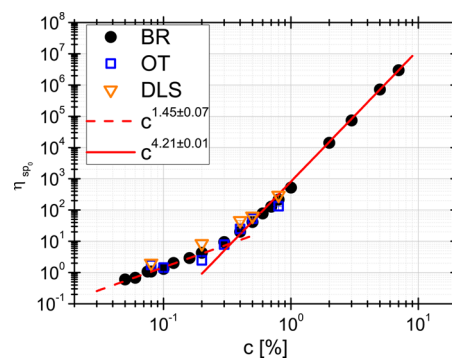

Figure 4. Specific viscosity η_{sp} versus HEC concentration measured using a conventional bulk rheology (BR, black circle), optical tweezers (OT, open blue square) and dynamic light scattering (DLS, open orange triangle). The red lines are the best fit of the BR experimental data.

At concentrations $c < 0.4$ wt%, the m-VROC derived measurements are not as accurate as at higher concentrations. This is because the test capillary with larger characteristic dimensions (i.e., height H and width W), required to investigate shear rates lower than $\dot{\gamma} \sim 10^3~s^{-1}$ (section 2.4.1), is not available in our lab.

In Figure 4, we show a comparison between the specific viscosity measured by applying three different rheological
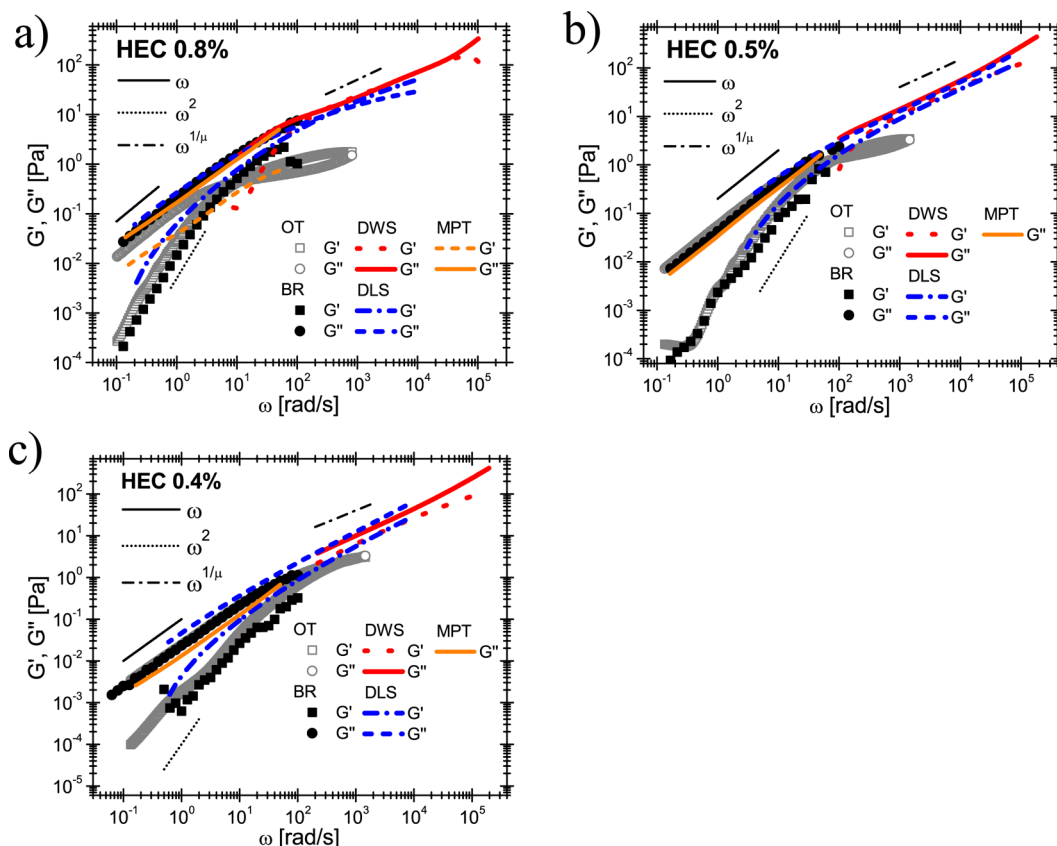
Figure 5. Comparison between the HEC solutions' linear viscoelastic moduli versus frequency measured with conventional rotational rheometer (BR), with optical tweezers (OT), Diffusive wave spectroscopy (DWS), Dynamic light scattering (DLS) and multiple particle tracking (MPT), for HEC solutions having concentrations of (a) 0.8, (b) 0.5, and (c) 0.4 wt%. The lines are guides for the theoretical predictions. Notice that $\mu = 1.76$[55,100] for all the concentrations investigated.

techniques for HEC solutions with concentration ranging from $c = 0.05$ wt% to $c = 7$ wt%. It is possible to identify two concentration regimes. For $c < 0.3$ wt%, the specific viscosity scales as $\eta_{sp_0} \propto c^{1.45\pm0.07}$ with a dimensionless exponent $\nu = 0.55 \pm 0.02$, evaluated via eq 10. These values are in good agreement with both the theoretical prediction for the semidilute unentangled regime of flexible polymers solutions,[55] and with the experimental evidence reported in the literature, both for polymers in good solvents[113] and for HEC solutions.[26,28] Whereas, the concentration functionality of the specific viscosity is significantly different from those predicted for rod-like polymers either in the dilute regime ($\eta_{sp_{0,D}} \propto c$) or in the semidilute regime ($\eta_{sp_{0,D}} \propto c^3$).

For $c > 0.3$ wt%, we found $\eta_{sp_0} \propto c^{4.21\pm0.01}$ with a dimensionless exponent $\nu = 0.57 \pm 0.08$. Both these values are in good agreement with theoretical predictions for flexible polymers suspended in good solvents and in the semidilute entangled regime.[55] Again, our experimental data at $c > 0.3$ wt% do not match any of the scalings reported for rod-like polymer solutions (see eq 12). Our viscosity measurements suggest that HEC in solutions behaves as a flexible polymer in good solvent, and not as a rod-like polymer, as observed elsewhere.[28] Notice that the value $\nu = 0.57$ derived from $\eta_{sp_0} \propto c^{4.21\pm0.01}$ should theoretically coincide with $\nu = 0.55$ derived from the previous extrapolation in the unentangled regime. We ascribe the slight discrepancy between those two values to the experimental uncertainty. Moreover, the viscosity values shown in Figure 4

are in quantitative agreement with those reported in literature.[23,25,26,28,114] However, while some studies[26,27,53,114] report the existence of two concentration regimes, as observed in this work, others report three regimes[23,28] over the same range of explored HEC concentrations. This discrepancy is ascribed to fitting of experimental data in the concentration range $0.05 < c < 0.3$ wt%. In fact, two polymer regimes can also be identified from our data set with scalings $\eta_{sp_0} \propto c^{0.64\pm0.06}$ for $0.05 < c < 0.1$ wt%, and $\eta_{sp_0} \propto c^{1.22\pm0.09}$ for $0.1 < c < 0.3$ wt% (data not shown). This identification would also be in agreement with an overlapping concentration $c^* = 0.1$ wt% derived[100] from our experimental data set as the concentration at which $\eta_{sp_0} = 1$. The exponent 0.64 of η_{sp_0} is close to the exponent of 2/5 predicted for polyelectrolytes in salt-free solutions.[55,115,116] However, above $c = 0.1$ wt%, the theoretical prediction for polyelectrolytes in the semidilute unentangled regime and in salt-free solutions is[55,115,116] $\eta_{sp_0} \propto c^{1/2}$, much weaker than that observed experimentally here, $\eta_{sp_0} \propto c^{1.22\pm0.09}$. In addition, we did not fit our data set with two separate scaling laws in the concentration range $0.05 < c < 0.3$ wt%, because a single scaling seemed adequate. Nevertheless, we cannot exclude the possibility that the *semidilute unentangled* regime spans a very narrow concentration range, e.g., $0.1 < c < 0.3$ wt%. From Figure 4, it is possible to identify the entanglement concentration as $c_e = 0.3$ wt%.

4.2. Linear Viscoelasticity. Before proceeding further, we would like to highlight the empirical Cox−Merz rule,[117] which
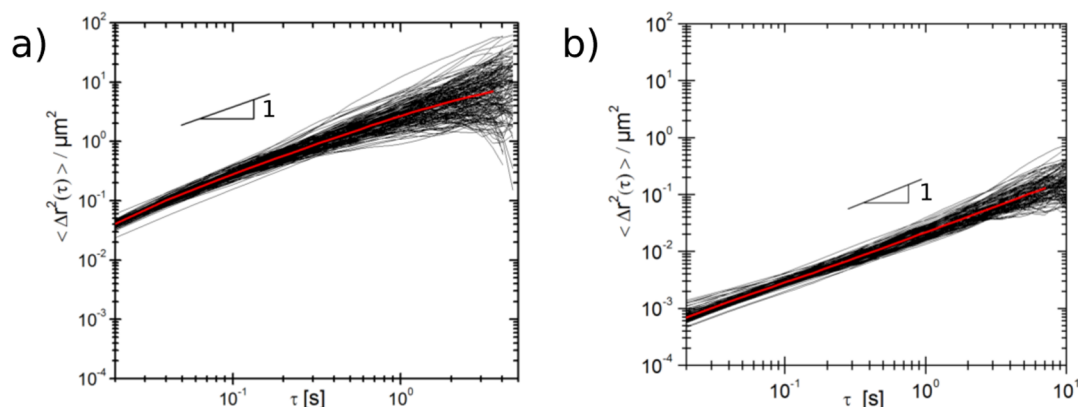
Figure 6. Mean square displacements (MSDs) of individual polystyrene microspheres of diameter 0.5 μm dispersed in HEC solutions of (a) 0.08 wt % and (b) 0.8 wt%. The red curve is the ensemble-average MSD. In both graphics, the black solid line represents a slope of one.

allows comparison of linear and nonlinear rheology results, as long as the latter are obtained from measurements that have reached a steady state. Here we compare our results obtained from bulk-, micro- and microfluidics-rheology techniques.

Some microrheology results are displayed in Figure 4, where the specific viscosity has been determined in terms of the fluid complex viscosity $|\eta^*(\omega)| = |G^*(\omega)|/\omega$ evaluated at vanishing low frequencies (i.e., in the fluid's terminal region where $G'(\omega) \propto \omega^2$ and $G''(\omega) \propto \omega$). Bulk rheology results (Figure 4) agree well with those obtained from two microrheology techniques (i.e., OT and DLS). Such agreement shows that micro-rheological techniques can be employed for the analysis of polymer solutions at low mass concentrations. Even though bulk rheology measurements alone can characterize the material, microrheological techniques can be employed for the rheological characterization of precious materials, where the available sample volume is relatively small and conventional techniques are not suitable.[38] On the other hand, for the characterization of polymer solutions at high mass concentrations, conventional bulk rheometry techniques are still preferable.

We now compare the frequency-dependent linear viscoelastic properties of the HEC solutions measured employing "five" different rheological techniques. In particular, we focus our attention on the frequency behavior of the viscoelastic moduli of three HEC solutions having concentrations higher than the entanglement concentration $c_e = 0.3$ wt%. Notwithstanding the quantitative agreement already shown in Figure 4 for HEC solutions at concentrations $c < c_e$, it was not always possible to measure both the moduli for such solutions with the techniques used, as it is still the case for MPT measurements when $c < 0.8$ wt% (Figure 5a−c).

Parts a−c of Figure 5 show the viscoelastic moduli $G'(\omega)$ and $G''(\omega)$ as a function of the angular frequency ω over more than 6 orders of magnitude in frequency. This is achieved by combining measurements performed with BR, OT, DWS, DLS, and MPT, for HEC solutions with three concentrations at 0.8, 0.5, and 0.4 wt%. The agreement among results from the five methods is apparent, though they explore different length scales and frequency ranges. Most remarkably, microrheology data obtained from DLS and DWS measurements have not been shifted vertically or horizontally, in contrast with other studies where a vertical shifting was applied.[111,112]

From Figures 5(a-c), the moduli show similar frequency behavior for all three HEC solutions. At low frequencies, the

moduli scale with frequency as $G'(\omega) \propto \omega^2$ and $G''(\omega) \propto \omega$, implying that the measurements are able to identify the material's terminal region, allowing λ extraction from the abscissa of the asymptotic crossover of the moduli. At high frequencies, microrheology measurements performed with DLS and DWS indicate that the moduli follow the theoretical prediction of linear flexible polymers, with $G'(\omega) \propto G''(\omega) \propto \omega^{1/\mu}$, where $\mu = 3\nu$ for the Zimm model, giving $\mu = {}^3/_2$ in dilute θ-solvents and $\mu = 1.76$ in good solvents.[55] Notably, the latter value is in quantitative agreement with $\mu = 1.75$ evaluated from $\nu = 0.57 \pm 0.08$ obtained from the viscosity scaling-law (Figure 4). Theoretical predictions for rod-like polymers would predict[99] $G'(\omega) \propto G''(\omega) \propto \omega^{3/4}$, which are significantly different form our findings. Hence, our linear viscoelasticity data follow the scalings for fully flexible polymers in good solvents and not those for rod-like polymers, in agreement with the findings reported in section 4.1.

We now discuss microrheology results obtained from optical tweezers (OT) and microparticle tracking (MPT). In the case of OT, while at low frequencies the results show good agreement with those obtained from bulk-rheology measurements, at high frequencies they seem to diverge from those obtained by using DLS and DWS. One possible cause could be the accuracy to which the displacement of the tracer is detected. Indeed, with regard to the bulk viscosity measurements (Figure 3) for an HEC solution at concentration of 0.4 wt%, the root-mean-square displacement (RMSD) of a 5 μm diameter particle at a frequency value of 100 rad/s is expected to be RMSD $= \sqrt{k_B T\tau/(6\pi\eta a)} \approx 6$ nm, which is very close to the camera resolution of the OT set up used in this work (i.e., on the order of a few nanometers[107]). Whereas, at low frequencies, i.e., at long lag-times τ, the particle has sufficient time to diffuse a distance much longer than the camera resolution, hence, a better agreement with the bulk-rheology measurements. A similar issue would occur also for the 0.4 μm tracers, but at much higher frequencies because they diffuse 12.5× faster than 5 μm tracers under the same experimental conditions.

MPT measurements have been performed in the frequency range $0.1 < \omega < 50$ rad/s. This upper value is limited by the acquisition rate of our camera, typically 50 frames per second in full-frame mode. For all samples investigated, we found that MPT is in quantitative agreement with BR, OT and DLS measurements. In particular, in the case of $G''(\omega)$, absolute values are in very good agreement among all the techniques. In the case of $G'(\omega)$, MPT is not able to detect its contribution to

particle diffusion, especially at low frequencies due to a loss of statistical information. Nevertheless, MPT provides useful information on microstructure around the Brownian tracer particles, as explained hereafter. Figure 6a and Figure 6b report two examples of MPT measurements performed on two HEC solutions at concentration of 0.08 wt% (in the unentangled regime) and 0.8 wt% (in the entangled regime). Both figures show the mean square displacements (MSDs) as a function of the lag-time for ~200 polystyrene particles of diameter 0.5 μm dispersed in the solutions. In Figure 6a, the MSDs exhibit a linear trend as a function of the lag-time ($\langle \Delta r^2(\tau) \rangle \sim \tau$), indicating that the motion of tracer particles is purely diffusive and that the microenvironment surrounding the particles responds like a viscous liquid. For the sample in the entangled regime (Figure 6b), MSD shows a power-law behavior as a function of the lag-time, with a slope slightly lower than one ($\langle \Delta r^2(\tau) \rangle \sim \tau^{0.85}$) in the time range $0.02 < \tau < 1$ s. This indicates that the motion of the particle is subdiffusive, which is the hallmark of viscoelastic behavior. At long times ($\tau > 1$ s), the slope of the MSDs increases slightly to reach almost a value of one, indicating the transition into the material's terminal regime.

Statistical analysis of MSD distributions in a van Hove diagram[109,110] reveals a homogeneous structure of the solution at μm length scale for all HEC concentrations explored, with a non-Gaussian parameter of $\alpha \sim 0$. This result contradicts the presence of heterogeneous μm-size structure (i.e., cellulose fibers) reported by Arfin and Bohidar.[28] With regard to measurement of viscoelastic moduli of all explored concentrations, a general qualitative agreement is found between MPT and bulk rheology (Figure 5a) for HEC solution at $c = 0.8$ wt%.

4.3. Longest Relaxation Time. In order to find λ from frequency-dependent viscoelastic moduli, we linearly extrapolated toward high frequencies (in a log–log plot) the characteristic scaling laws of the moduli within the fluids' terminal region (i.e., $G'(\omega) \propto \omega^2$ and $G''(\omega) \propto \omega$). The abscissa of the intercept between the two straight lines provides a measure of the longest relaxation time λ.[31] Notice that, this is a common procedure that only applies when the terminal region of the fluid is clearly identified, which is a nontrivial condition in the case of bulk-rheology, especially for weakly viscoelastic fluids.[35] As an alternative, Del Giudice et al.[51] proposed a novel microfluidic platform for measuring λ (down to microseconds[52]) of any (weakly viscoelastic) polymer solution.

In Figure 7, we report the values of λ obtained from "five" rheological techniques. The agreement among these results is very good, apart from those obtained via the Bird–Carreau model,[89] which provides lower values of λ when compared with the other techniques.

By considering the same two HEC concentration regimes identified while analyzing solution specific viscosity, we fit λ with both eq 10 and eq 11 for $c < c_e = 0.3$ wt% and $c > c_e = 0.3$ wt%, respectively. For concentration values $c < c_e$ we found that $\lambda \propto c^{0.58 \pm 0.06}$, which is in good agreement with the theoretical prediction for flexible polymers with $\nu = 0.55$ (in a rather good solvent), and consistent with our previous estimate of $\nu = 0.55$ from specific viscosity measures (Figure 4). For concentration values $c > c_e$ (semidilute entangled regime), the fitting procedure provides a concentration dependence of $\lambda \propto c^{4.18 \pm 0.12}$, the power law index being higher than theoretical values,[55] $\lambda_{theo} \propto c^{1.6}$. Nevertheless, the exponent value of 4.18 is in good agreement with that reported by Haward et al.[105] (3.8)
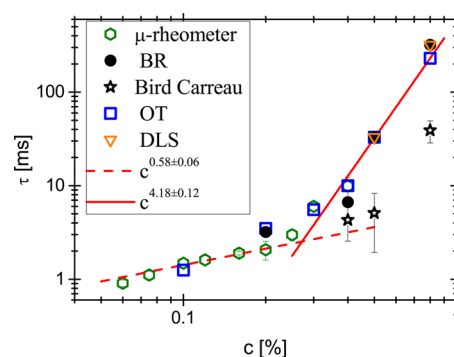

Figure 7. Comparison between the HEC solutions' longest shear relaxation time λ, directly measured with a μ-rheometer and those educed from viscoelastic moduli measured by means of a rotational rheometer, dynamic light scattering and optical tweezers. The concentration c is expressed in wt%. Lines are the concentration scaling laws of λ, as described in the text.

in the case of extensional rheology of a hydrophobically modified cellulose in an ionic liquid. They attributed the higher value of the exponent to the high degree of molecular interactions caused by the chain stretching.[113,118] Another possible explanation for the discrepancy between the experimental and theoretical values of the exponents could be due to the formation of aggregates at higher HEC concentrations, as also reported by Arfin and Bohidar.[28] Aggregation is presumably caused by the formation of hydrogen bonds between HEC chains, which is more likely to happen at higher concentrations. A similar trend has also been observed for hyaluronic acid solutions (HA) in the entangled regime,[119] and possibly due to the existence of HA associations or microgels, suggested by scattering measurements.[120] Such aggregates should occur on length scales <1 μm, since our MPT measurements assured local homogeneity on length scales ≥1 μm. The disagreement between concentration scaling laws of the viscosity and the relaxation time (for the semidilute entangled regime found in this work) has been observed for polymer solutions. Clasen et al.[118] found that, even in the dilute regime, the concentration scaling law of the specific viscosity was in agreement with the theoretical predictions, while the relaxation time was not described by the same theoretical model.

5. CONCLUSIONS

In this work, we have performed an extensive rheological investigation of both the linear and nonlinear rheology of unmodified hydroxyethyl cellulose aqueous solutions to provide new insights into the debate on the morphological structure of HEC molecules when dissolved in water. We have employed "seven" rheological techniques to explore viscoelastic properties of HEC solutions with $0.05 < c < 8$ wt%, at different time and length scales. We have used (i) a stress-controlled rotational rheometer to perform conventional bulk-rheology measurements and four microrheology methods including (ii) optical tweezers, (iii) diffusing wave spectroscopy, (iv) dynamic light scattering, (v) passive video particle tracking, and two microfluidics platforms (vi) m-VROC and (vii) μ-rheometer. The results of all these techniques display remarkable and 'rarely seen' agreement, making the outcomes of this work 'self-consistent'. Our results are in good agreement with theoretical predictions for flexible polymers solutions.[55] In particular, we have found that (i) when dissolved in water, unmodified

hydroxyethyl cellulose behaves like a linear uncharged polymer with an entangled mass concentration equal to $c_e = 0.3$ wt%. (ii) The $c < c_e$ concentration scaling laws of the solution specific viscosity and their longest shear shear relaxation time are $\eta_{sp} \propto c^{1.45\pm0.07}$ and $\lambda \propto c^{0.58\pm0.06}$, respectively. (iii) For $c > c_e$, concentration scaling laws become $\eta_{sp} \propto c^{4.21\pm0.01}$ and $\lambda \propto c^{4.18\pm0.12}$, respectively. Finally, to the best of our knowledge, this is the *first time* that concentration scaling laws of λ have been derived from direct measurements (μ-rheometer, bulk rheology, optical tweezers, and dynamic light scattering) rather then being inferred from semiempirical theoretical models where λ is used as a fitting parameter of fluid shear flow curves, such as in the Bird–Carreau model.[89]

■ AUTHOR INFORMATION

Corresponding Authors

*(F.D.G.) E-mail: francesco.delgiudice@me.com.
*(M.T.) E-mail: manlio.tassieri@glasgow.ac.uk.

ORCID

Francesco Del Giudice: 0000-0002-9414-6937
Manlio Tassieri: 0000-0002-6807-0385

Notes

The authors declare no competing financial interest.

■ ACKNOWLEDGMENTS

■ REFERENCES

(1) Naik, S. C. When Microrheology, Bulk Rheology, and Microfluidics Meet: Broadband Rheology of Hydroxyethyl Cellulose Water Solutions. *Trans. Soc. Rheol.* **1976**, *20*, 639−649.

(2) Lu, S.; Forcada, J. Preparation and characterization of magnetic polymeric composite particles by miniemulsion polymerization. *J. Polym. Sci., Part A: Polym. Chem.* **2006**, *44*, 4187−4203.

(3) Sehaqui, H.; Morimune, S.; Nishino, T.; Berglund, L. A. Stretchable and strong cellulose nanopaper structures based on polymer-coated nanofiber networks: An alternative to nonwoven porous membranes from electrospinning. *Biomacromolecules* **2012**, *13*, 3661−3667.

(4) Zhou, Z.; Zheng, H.; Wei, M.; Huang, J.; Chen, Y. Structure and mechanical properties of cellulose derivatives/soy protein isolate blends. *J. Appl. Polym. Sci.* **2008**, *107*, 3267−3274.

(5) Cheroni, S.; Gatti, B.; Margheritis, G.; Formantici, C.; Perrone, L.; Galante, Y. Enzyme resistance and biostability of hydroxyalkylated cellulose and galactomannan as thickeners in waterborne paints. *Int. Biodeterior. Biodegrad.* **2012**, *69*, 106−112.

(6) Wetzel, W. H.; Chen, M.; Glass, J. E. *Adv. Chem. Ser.* **1996**, *248*, 163−179.

(7) Tanaka, R.; Meadows, J.; Williams, P.; Phillips, G. Interaction of hydrophobically modified hydroxyethyl cellulose with various added surfactants. *Macromolecules* **1992**, *25*, 1304−1310.

(8) Kästner, U. The impact of rheological modifiers on water-borne coatings. *Colloids Surf., A* **2001**, *183-185*, 805−821.

(9) Maestro, A.; González, C.; Gutierrez, J. M. Interaction of surfactants with thickeners used in waterborne paints: A rheological study. *J. Colloid Interface Sci.* **2005**, *288*, 597−605.

(10) Xu, X.; Zhuang, X.; Cheng, B.; Xu, J.; Long, G.; Zhang, H. Manufacture and properties of cellulose/O-hydroxyethyl chitosan blend fibers. *Carbohydr. Polym.* **2010**, *81*, 541−544.

(11) Chanachai, A.; Jiraratananon, R.; Uttapap, D.; Moon, G.; Anderson, W.; Huang, R. Pervaporation with chitosan/hydroxyethyl-cellulose (CS/HEC) blended membranes. *J. Membr. Sci.* **2000**, *166*, 271−280.

(12) Beeskow, T.; Kusharyoto, W.; Anspach, F.; Kroner, K.; Deckwer, W.-D. Surface modification of microporous polyamide membranes with hydroxyethyl cellulose and their application as affinity membranes. *J. Chromatogr A* **1995**, *715*, 49−65.

(13) Anders, R.; Merkle, H. P. Evaluation of laminated muco-adhesive patches for buccal drug delivery. *Int. J. Pharm.* **1989**, *49*, 231−240.

(14) Zheng, Y.; Yao, G.; Cheng, Q.; Yu, S.; Liu, M.; Gao, C. Positively charged thin-film composite hollow fiber nanofiltration membrane for the removal of cationic dyes through submerged filtration. *Desalination* **2013**, *328*, 42−50.

(15) Rodríguez, R.; Alvarez-Lorenzo, C.; Concheiro, A. Cationic cellulose hydrogels: kinetics of the cross-linking process and characterization as pH-/ion-sensitive drug delivery systems. *J. Controlled Release* **2003**, *86*, 253−265.

(16) Kamel, S.; Ali, N.; Jahangir, K.; Shah, S.; El-Gendy, A. Pharmaceutical significance of cellulose: a review. *eXPRESS Polym. Lett.* **2008**, *2*, 758−778.

(17) Baumgartner, S.; Kristl, J.; Peppas, N. A. Network structure of cellulose ethers used in pharmaceutical applications during swelling and at equilibrium. *Pharm. Res.* **2002**, *19*, 1084−1090.

(18) Angadi, S. C.; Manjeshwar, L. S.; Aminabhavi, T. M. Interpenetrating polymer network blend microspheres of chitosan and hydroxyethyl cellulose for controlled release of isoniazid. *Int. J. Biol. Macromol.* **2010**, *47*, 171−179.

(19) Miyamoto, T.; Takahashi, S.; Ito, H.; Inagaki, H.; Noishiki, Y. Tissue biocompatibility of cellulose and its derivatives. *J. Biomed. Mater. Res.* **1989**, *23*, 125−133.

(20) Hao, T.; Wen, N.; Cao, J.-K.; Wang, H.-B.; Lü, S.-H.; Liu, T.; Lin, Q.-X.; Duan, C.-M.; Wang, C.-Y. The support of matrix accumulation and the promotion of sheep articular cartilage defects repair in vivo by chitosan hydrogels. *Osteoarthr Cartilage* **2010**, *18*, 257−265.

(21) Hoemann, C.; Chenite, A.; Sun, J.; Hurtig, M.; Serreqi, A.; Lu, Z.; Rossomacha, E.; Buschmann, M. Cytocompatible gel formation of chitosan-glycerol phosphate solutions supplemented with hydroxyl ethyl cellulose is due to the presence of glyoxal. *J. Biomed. Mater. Res., Part A* **2007**, *83A*, 521−529.

(22) Chen, D.; Sun, B. New tissue engineering material copolymers of derivatives of cellulose and lactide: their synthesis and characterization. *Mater. Sci. Eng., C* **2000**, *11*, 57−60.

(23) Meadows, J.; Williams, P. A.; Kennedy, J. C. Comparison of the extensional and shear viscosity characteristics of aqueous hydroxyethyl cellulose solutions. *Macromolecules* **1995**, *28*, 2683−2692.

(24) Maestro, A.; Gonzalez, C.; Gutierrez, J. M. Shear thinning and thixotropy of HMHEC and HEC water solutions. *J. Rheol.* **2002**, *46*, 1445−1457.

(25) Laschet, M.; Plog, J. P.; Clasen, C.; Kulicke, W.-M. Examination of the flow behaviour of HEC and hmHEC solutions using structure−property relationships and rheo-optical methods. *Colloid Polym. Sci.* **2004**, *282*, 373−380.

(26) Castelain, C.; Doublier, J.; Lefebvre, J. A study of the viscosity of cellulose derivatives in aqueous solutions. *Carbohydr. Polym.* **1987**, *7*, 1−16.

(27) Kästner, U.; Hoffmann, H.; Dönges, R.; Ehrler, R. Hydrophobically and cationically modified hydroxyethyl cellulose and their interactions with surfactants. *Colloids Surf., A* **1994**, *82*, 279−297.

(28) Arfin, N.; Bohidar, H. Concentration selective hydration and phase states of hydroxyethyl cellulose (HEC) in aqueous solutions. *Int. J. Biol. Macromol.* **2012**, *50*, 759−767.

(29) Doi, M.; Edwards, S. F. Dynamics of rod-like macromolecules in concentrated solution. Part 1. *J. Chem. Soc., Faraday Trans. 2* **1978**, *74*, 560.

(30) Doi, M.; Edwards, S. F. Dynamics of rod-like macromolecules in concentrated solution. Part 2. *J. Chem. Soc., Faraday Trans. 2* **1978**, *74*, 918.

(31) Macosko, C. *Rheology: Principles, measurements, and applications*; Wiley-VCH: 1994.

(32) Brau, R. R.; Ferrer, J. M.; Lee, H.; Castro, C. E.; Tam, B. K.; Tarsa, P. B.; Matsudaira, P.; Boyce, M. C.; Kamm, R. D.; Lang, M. J. Passive and active microrheology with optical tweezers. *J. Opt. A: Pure Appl. Opt.* **2007**, *9*, S103−S112.

(33) Fischer, M.; Berg-Sørensen, K. Calibration of trapping force and response function of optical tweezers in viscoelastic media. *J. Opt. A: Pure Appl. Opt.* **2007**, *9*, S239−S250.

(34) Atakhorrami, M.; Sulkowska, J. I.; Addas, K. M.; Koenderink, G. H.; Tang, J. X.; Levine, A. J.; MacKintosh, F. C.; Schmidt, C. F. Correlated fluctuations of microparticles in viscoelastic solutions: Quantitative measurement of material properties by microrheology in the presence of optical traps. *Phys. Rev. E* **2006**, *73*, 061501.

(35) Pommella, A.; Preziosi, V.; Caserta, S.; Cooper, J. M.; Guido, S.; Tassieri, M. Using Optical Tweezers for the Characterization of Polyelectrolyte Solutions with Very Low Viscoelasticity. *Langmuir* **2013**, *29*, 9224−9230.

(36) Watts, F.; Tan, L. E.; Wilson, C. G.; Girkin, J. M.; Tassieri, M.; Wright, A. J. Investigating the micro-rheology of the vitreous humor using an optically trapped local probe. *J. Opt.* **2014**, *16*, 015301.

(37) Lee, M. P.; Curran, A.; Gibson, G. M.; Tassieri, M.; Heckenberg, N. R.; Padgett, M. J. Optical shield: measuring viscosity of turbid fluids using optical tweezers. *Opt. Express* **2012**, *20*, 12127.

(38) Tassieri, M.; Del Giudice, F.; Robertson, E. J.; Jain, N.; Fries, B.; Wilson, R.; Glidle, A.; Greco, F.; Netti, P. A.; Maffettone, P. L.; Bicanic, T.; Cooper, J. M. Microrheology with Optical Tweezers: Measuring the relative viscosity of solutions 'at a glance'. *Sci. Rep.* **2015**, *5*, 8831.

(39) Pine, D. J.; Weitz, D. A.; Chaikin, P. M.; Herbolzheimer, E. Diffusing wave spectroscopy. *Phys. Rev. Lett.* **1988**, *60*, 1134−1137.

(40) Weitz, D. A.; Zhu, J. X.; Durian, D. J.; Gang, H.; Pine, D. J. Diffusing-wave spectroscopy: The technique and some applications. *Phys. Scr.* **1993**, *T49B*, 610−621.

(41) Waigh, T. A. Microrheology of complex fluids. *Rep. Prog. Phys.* **2005**, *68*, 685−742.

(42) Berne, B. J.; Pecora, R. *Dynamic light scattering: with applications to chemistry, biology, and physics*; Courier Corporation: 1976.

(43) Apgar, J.; Tseng, Y.; Fedorov, E.; Herwig, M. B.; Almo, S. C.; Wirtz, D. Multiple-particle tracking measurements of heterogeneities in solutions of actin filaments and actin bundles. *Biophys. J.* **2000**, *79*, 1095−1106.

(44) Ma, L.; Yamada, S.; Wirtz, D.; Coulombe, P. A. A 'hot-spot' mutation alters the mechanical properties of keratin filament networks. *Nat. Cell Biol.* **2001**, *3*, 503−506.

(45) Mason, T.; Ganesan, K.; Van Zanten, J.; Wirtz, D.; Kuo, S. Particle tracking microrheology of complex fluids. *Phys. Rev. Lett.* **1997**, *79*, 3282.

(46) Kowalczyk, A.; Oelschlaeger, C.; Willenbacher, N. Tracking errors in 2D multiple particle tracking microrheology. *Meas. Sci. Technol.* **2015**, *26*, 015302.

(47) Kowalczyk, A.; Oelschlaeger, C.; Willenbacher, N. Visualization of micro-scale inhomogeneities in acrylic thickener solutions: A multiple particle tracking study. *Polymer* **2015**, *58*, 170−179.

(48) Oelschlaeger, C.; Bossler, F.; Willenbacher, N. Synthesis, Structural and Micromechanical Properties of 3D Hyaluronic Acid-Based Cryogel Scaffolds. *Biomacromolecules* **2016**, *17*, 580−589.

(49) Pipe, C. J.; Majmudar, T. S.; McKinley, G. H. High shear rate viscometry. *Rheol. Acta* **2008**, *47*, 621−642.

(50) Pipe, C. J.; McKinley, G. H. Microfluidic rheometry. *Mech. Res. Commun.* **2009**, *36*, 110−120.

(51) Del Giudice, F.; D'Avino, G.; Greco, F.; De Santo, I.; Netti, P. A.; Maffettone, P. L. Rheometry-on-a-chip: measuring the relaxation time of a viscoelastic liquid through particle migration in microchannel flows. *Lab Chip* **2015**, *15*, 783−792.

(52) Del Giudice, F.; Calcagno, V.; Esposito Taliento, V.; Greco, F.; Netti, P. A.; Maffettone, P. L. Relaxation time of polyelectrolyte solutions: when μ-rheometry steps in charge. *J. Rheol.* **2017**, *61*, 13−21.

(53) Hoffmann, H.; Kästner, U.; Dönges, R.; Ehrler, R. Gels from modified hydroxyethyl cellulose and ionic surfactants. *Polym. Gels Networks* **1996**, *4*, 509−526.

(54) Ishii, D.; Saito, T.; Isogai, A. Viscoelastic Evaluation of Average Length of Cellulose Nanofibers Prepared by TEMPO-Mediated Oxidation. *Biomacromolecules* **2011**, *12*, 548−550.

(55) Colby, R. H. Structure and linear viscoelasticity of flexible polymer solutions: comparison of polyelectrolyte and neutral polymer solutions. *Rheol. Acta* **2010**, *49*, 425−442.

(56) Simha, R.; Zakin, J. L. Solution viscosities of linear flexible high polymers. *J. Colloid Sci.* **1962**, *17*, 270−287.

(57) Saito, T.; Kimura, S.; Nishiyama, Y.; Isogai, A. Cellulose Nanofibers Prepared by TEMPO-Mediated Oxidation of Native Cellulose. *Biomacromolecules* **2007**, *8*, 2485−2491.

(58) Tanaka, R.; Saito, T.; Ishii, D.; Isogai, A. Determination of nanocellulose fibril length by shear viscosity measurement. *Cellulose* **2014**, *21*, 1581−1589.

(59) Jowkarderis, L.; van de Ven, T. G. Intrinsic viscosity of aqueous suspensions of cellulose nanofibrils. *Cellulose* **2014**, *21*, 2511−2517.

(60) Lu, A.; Hemraz, U.; Khalili, Z.; Boluk, Y. Unique viscoelastic behaviors of colloidal nanocrystalline cellulose aqueous suspensions. *Cellulose* **2014**, *21*, 1239−1250.

(61) Nazari, B.; Kumar, V.; Bousfield, D. W.; Toivakka, M. Rheology of cellulose nanofibers suspensions: Boundary driven flow. *J. Rheol.* **2016**, *60*, 1151−1159.

(62) Mason, T. G.; Weitz, D. A. Optical Measurements of Frequency-Dependent Linear Viscoelastic Moduli of Complex Fluids. *Phys. Rev. Lett.* **1995**, *74*, 1250−1253.

(63) Mason, T. G. Estimating the viscoelastic moduli of complex fluids using the generalized Stokes-Einstein equation. *Rheol. Acta* **2000**, *39*, 371−378.

(64) de Gennes, P. G. Reptation of a Polymer Chain in the Presence of Fixed Obstacles. *J. Chem. Phys.* **1971**, *55*, 572.

(65) McLeish, T. C. B. Tube theory of entangled polymer dynamics. *Adv. Phys.* **2002**, *51*, 1379−1527.

(66) Ferry, J. D. *Viscoelastic properties of polymers*; John Wiley & Sons: 1980.

(67) Tassieri, M.; Laurati, M.; Curtis, D. J.; Auhl, D. W.; Coppola, S.; Scalfati, A.; Hawkins, K.; Williams, P. R.; Cooper, J. M. i-Rheo: Measuring the materials' linear viscoelastic properties 'in a step'! *J. Rheol.* **2016**, *60*, 649−660.

(68) Tassieri, M.; Evans, R. M. L.; Barbu-Tudoran, L.; Khaname, G. N.; Trinick, J.; Waigh, T. A. Dynamics of Semiflexible Polymer Solutions in the Highly Entangled Regime. *Phys. Rev. Lett.* **2008**, *101*, 198301.

(69) Waigh, T. A. Advances in the microrheology of complex fluids. *Rep. Prog. Phys.* **2016**, *79*, 074601.

(70) Gupta, S.; Wang, W. S.; Vanapalli, S. A. Microfluidic viscometers for shear rheology of complex fluids and biofluids. *Biomicrofluidics* **2016**, *10*, 043402.

(71) Kuo, S. C.; Gelles, J.; Steuer, E.; Sheetz, M. P. A model for kinesin movement from nanometer-level movements of kinesin and cytoplasmic dynein and force measurements. *J. Cell Sci.* **1991**, *1991*, 135−138.

(72) Valentine, M. T.; Kaplan, P. D.; Thota, D.; Crocker, J. C.; Gisler, T.; Prud'homme, R. K.; Beck, M.; Weitz, D. A. Investigating the microenvironments of inhomogeneous soft materials with multiple particle tracking. *Phys. Rev. E: Stat. Phys., Plasmas, Fluids, Relat. Interdiscip. Top.* **2001**, *64*, 061506.

(73) Bausch, A. R.; Möller, W.; Sackmann, E. Measurement of Local Viscoelasticity and Forces in Living Cells by Magnetic Tweezers. *Biophys. J.* **1999**, *76*, 573−579.

(74) Tassieri, M.; Waigh, T. A.; Trinick, J.; Aggeli, A.; Evans, R. M. L. Analysis of the linear viscoelasticity of polyelectrolytes by magnetic microrheometry—Pulsed creep experiments and the one particle response. *J. Rheol.* **2010**, *54*, 117−131.

(75) Tassieri, M.; Gibson, G. M.; Evans, R. M. L.; Yao, A. M.; Warren, R.; Padgett, M. J.; Cooper, J. M. Measuring storage and loss moduli using optical tweezers: Broadband microrheology. *Phys. Rev. E* **2010**, *81*, 026308.

(76) Dasgupta, B. R.; Tee, S.-Y.; Crocker, J. C.; Frisken, B. J.; Weitz, D. A. Microrheology of polyethylene oxide using diffusing wave spectroscopy and single scattering. *Phys. Rev. E: Stat. Phys., Plasmas, Fluids, Relat. Interdiscip. Top.* **2002**, *65*, 051505.

(77) Okajima, T.; Tokumoto, H. Nanorheology of living cells investigated by atomic force microscopy. *Nihon Reoroji Gakk* **2008**, *36*, 81−86.

(78) Tripathy, S.; Berger, E. J. Measuring Viscoelasticity of Soft Samples Using Atomic Force Microscopy. *J. Biomech. Eng.* **2009**, *131*, 094507.

(79) Squires, T. M.; Mason, T. G. Fluid Mechanics of Microrheology. *Annu. Rev. Fluid Mech.* **2010**, *42*, 413−438.

(80) He, J.; Mak, M.; Liu, Y.; Tang, J. X. Counterion-dependent microrheological properties of F-actin solutions across the isotropic-nematic phase transition. *Phys. Rev. E* **2008**, *78*, 011908.

(81) Addas, K. M.; Schmidt, C. F.; Tang, J. X. Microrheology of solutions of semiflexible biopolymer filaments using laser tweezers interferometry. *Phys. Rev. E* **2004**, *70*, 021503.

(82) Atakhorrami, M.; Mizuno, D.; Koenderink, G.; Liverpool, T.; MacKintosh, F.; Schmidt, C. Short-time inertial response of viscoelastic fluids measured with Brownian motion and with active probes. *Phys. Rev. E* **2008**, *77*, 061508.

(83) Moschakis, T.; Murray, B. S.; Dickinson, E. Particle tracking using confocal microscopy to probe the microrheology in a phase-separating emulsion containing nonadsorbing polysaccharide. *Langmuir* **2006**, *22*, 4710−4719.

(84) Moschakis, T.; Murray, B. S.; Dickinson, E. On the kinetics of acid sodium caseinate gelation using particle tracking to probe the microrheology. *J. Colloid Interface Sci.* **2010**, *345*, 278−285.

(85) Cheng, Z.; Mason, T. Rotational diffusion microrheology. *Phys. Rev. Lett.* **2003**, *90*, 018304.

(86) Tassieri, M.; Evans, R. M. L.; Warren, R. L.; Bailey, N. J.; Cooper, J. M. Microrheology with optical tweezers: data analysis. *New J. Phys.* **2012**, *14*, 115032.

(87) Tassieri, M. Linear microrheology with optical tweezers of living cells 'is not an option'! *Soft Matter* **2015**, *11*, 5792−5798.

(88) Preece, D.; Warren, R.; Evans, R. M. L.; Gibson, G. M.; Padgett, M. J.; Cooper, J. M.; Tassieri, M. Optical tweezers: wideband microrheology. *J. Opt.* **2011**, *13*, 044022.

(89) Bird, R. B.; Carreau, P. J. A nonlinear viscoelastic model for polymer solutions and melts—I. *Chem. Eng. Sci.* **1968**, *23*, 427−434.

(90) Zilz, J.; Schäfer, C.; Wagner, C.; Poole, R. J.; Alves, M. A.; Lindner, A. Serpentine channels: micro-rheometers for fluid relaxation times. *Lab Chip* **2014**, *14*, 351−358.

(91) Del Giudice, F.; Romeo, G.; D'Avino, G.; Greco, F.; Netti, P. A.; Maffettone, P. L. Particle alignment in a viscoelastic liquid flowing in a square-shaped microchannel. *Lab Chip* **2013**, *13*, 4263.

(92) Leshansky, A.; Bransky, A.; Korin, N.; Dinnar, U. Tunable nonlinear viscoelastic "focusing" in a microfluidic device. *Phys. Rev. Lett.* **2007**, *98*, 234501.

(93) Yang, S.; Kim, J. Y.; Lee, S. J.; Lee, S. S.; Kim, J. M. Sheathless elasto-inertial particle focusing and continuous separation in a straight rectangular microchannel. *Lab Chip* **2011**, *11*, 266−273.

(94) D'Avino, G.; Romeo, G.; Villone, M. M.; Greco, F.; Netti, P. A.; Maffettone, P. L. Single line particle focusing induced by viscoelasticity of the suspending liquid: theory, experiments and simulations to design a micropipe flow-focuser. *Lab Chip* **2012**, *12*, 1638−1645.

(95) Del Giudice, F.; D'Avino, G.; Greco, F.; Netti, P. A.; Maffettone, P. L. Effect of fluid rheology on particle migration in a square-shaped microchannel. *Microfluid. Nanofluid.* **2015**, *19*, 95−104.

(96) Bretherton, F. P. The motion of rigid particles in a shear flow at low Reynolds number. *J. Fluid Mech.* **1962**, *14*, 284−304.

(97) Romeo, G.; D'Avino, G.; Greco, F.; Netti, P. A.; Maffettone, P. L. Viscoelastic flow-focusing in microchannels: scaling properties of the particle radial distributions. *Lab Chip* **2013**, *13*, 2802−2807.

(98) Doi, M.; Edwards, S. F. *The theory of polymer dynamics*; Oxford University Press: 1988; Vol. 73.

(99) Morse, D. C. Viscoelasticity of concentrated isotropic solutions of semiflexible polymers. 2. Linear response. *Macromolecules* **1998**, *31*, 7044−7067.

(100) Rubinstein, M.; Colby, R. *Polymers Physics*; Oxford: 2003.

(101) Schuldt, C.; Schnauß, J.; Händler, T.; Glaser, M.; Lorenz, J.; Golde, T.; Käs, J. A.; Smith, D. M. Tuning Synthetic Semiflexible Networks by Bending Stiffness. *Phys. Rev. Lett.* **2016**, *117*, 197801.

(102) Wyatt, P. J. Light scattering and the absolute characterization of macromolecules. *Anal. Chim. Acta* **1993**, *272*, 1−40.

(103) Vadodaria, S. S.; English, R. J. Aqueous solutions of HEC and hmHEC: effects of molecular mass versus hydrophobic associations on hydrodynamic and thermodynamic parameters. *Cellulose* **2016**, *23*, 1107−1121.

(104) Brown, W.; Henley, D.; Öhman, J. Studies on cellulose derivatives. Part II. The influence of solvent and temperature on the configuration and hydrodynamic behaviour of hydroxyethyl cellulose in dilute solution. *Makromol. Chem.* **1963**, *64*, 49−67.

(105) Haward, S. J.; Sharma, V.; Butts, C. P.; McKinley, G. H.; Rahatekar, S. S. Shear and extensional rheology of cellulose/ionic liquid solutions. *Biomacromolecules* **2012**, *13*, 1688−1699.

(106) Dumitriu, S. *Polysaccharides: structural diversity and functional versatility*; CRC Press: 2004.

(107) Gibson, G. M.; Leach, J.; Keen, S.; Wright, A. J.; Padgett, M. J. Measuring the accuracy of particle position and force in optical tweezers using high-speed video microscopy. *Opt. Express* **2008**, *16*, 14561.

(108) Crocker, J. C.; Grier, D. G. Methods of digital video microscopy for colloidal studies. *J. Colloid Interface Sci.* **1996**, *179*, 298−310.

(109) Van Hove, L. Correlations in space and time and Born approximation scattering in systems of interacting particles. *Phys. Rev.* **1954**, *95*, 249.

(110) Weeks, E. R.; Crocker, J. C.; Levitt, A. C.; Schofield, A.; Weitz, D. A. Three-dimensional direct imaging of structural relaxation near the colloidal glass transition. *Science* **2000**, *287*, 627−631.

(111) Reufer, M. *DWS Microrheology of Aqueous Polymer Solutions*; LS Instruments: 2015

(112) Oelschlaeger, C.; Schopferer, M.; Scheffold, F.; Willenbacher, N. Linear-to-branched micelles transition: A rheometry and diffusing wave spectroscopy (DWS) study. *Langmuir* **2009**, *25*, 716−723.

(113) Tirtaatmadja, V.; McKinley, G. H.; Cooper-White, J. J. Drop formation and breakup of low viscosity elastic fluids: Effects of molecular weight and concentration. *Phys. Fluids* **2006**, *18*, 043101.

(114) Tanaka, R.; Meadows, J.; Phillips, G.; Williams, P. Viscometric and spectroscopic studies on the solution behaviour of hydrophobically modified cellulosic polymers. *Carbohydr. Polym.* **1990**, *12*, 443−459.

(115) Dobrynin, A. V.; Colby, R. H.; Rubinstein, M. Scaling theory of polyelectrolyte solutions. *Macromolecules* **1995**, *28*, 1859−1871.

(116) Dubrovskii, S.; Zelenetskii, A.; Uspenskii, S.; Khabarov, V. Effect of borax additives on the rheological properties of sodium hyaluronate aqueous solutions. *Polym. Sci., Ser. A* **2014**, *56*, 205−210.

(117) Cox, W. P.; Merz, E. H. Correlation of dynamic and steady flow viscosities. *J. Polym. Sci.* **1958**, *28*, 619−622.

(118) Clasen, C.; Plog, J. P.; Kulicke, W.-M.; Owens, M.; Macosko, C.; Scriven, L. E.; Verani, M.; McKinley, G. H. How dilute are dilute solutions in extensional flows? *J. Rheol.* **2006**, *50*, 849.

(119) Oelschlaeger, C.; Cota Pinto Coelho, M.; Willenbacher, N. Chain flexibility and dynamics of polysaccharide hyaluronan in entangled solutions: a high frequency rheology and diffusing wave spectroscopy study. *Biomacromolecules* **2013**, *14*, 3689−3696.

(120) Esquenet, C.; Buhler, E. Aggregation behavior in semidilute rigid and semirigid polysaccharide solutions. *Macromolecules* **2002**, *35*, 3708−3716.